Mobile multiwave lidar complexes

A.S. Boreysho, M.A. Konyaev, A.V. Morozov, A.V. Pikulik,
A.V. Savin, A.V. Trilis, S.Ya. Chakchir, N.I. Boiko,
Yu.N. Vlasov, S.P. Nikitaev, A.V. Rozhnov

Abstract. **Multiwave mobile lidar complexes (MLCs) are designed and developed. A number of vehicle-based MLCs are built. The set of complex lidar probing data obtained with the help of MLCs is synchronised in space and time, covers a large area (the operation range of an MLC is 15 km), and is based on a unified methodological approach. The results of probing contain information on the concentration and physical nature of atmospheric aerosol, chemical composition of the gaseous phase of the atmosphere, wind and turbulence. The obtained data form the basis for a complex analysis of the ecological situation and prognosis of its development.**

Keywords: *heterodyne lidar, differential probing, single-frequency laser, laser-induced fluorescence*

1. Introduction

The task of monitoring the environment requires complex means that would provide along with monitoring over a wide region of space also detailed information on various meteorological and ecological parameters of the atmosphere state. Remote lidar monitoring technologies [1] offer the broadest possibilities of collecting data about the concentration of contaminating substances in the atmosphere, wind velocity distribution and turbulence parameters. However, a complex analysis of the ecological situation imposes special requirements on the composition and structure of the lidar system, and a solution of these problems requires a combination of a whole range of such technologies using a unified methodological approach.

To analyse and predict the ecological situation as a whole, it is necessary to match all the obtained data in space both in covered regions and spatial resolution, to synchronise them in time, and present them in the same format and the same methodological basis. Modern software and

A.S. Boreysho, M.A. Konyaev, A.V. Morozov, A.V. Pikulik, A.V. Savin, A.V. Trilis, S.Ya. Chakchir Institute of Laser Technics and Technology D.F. Ustinov Baltic State Technical University 'Voenmekh', Laser Systems Ltd, 1-ya Krasnoarmeiskaya ul. 1, 198005 St. Petersburg, Russia; e-mail: office@lsystems.ru;
N.I. Boiko, Yu.N. Vlasov, S.P. Nikitaev, A.V. Rozhnov Administration of the Commander of Radiation, Chemical and Biological Defence Corps of the Armed Forces of the Russian Federation, Frunzenskaya nab. 22/2, 119160 Moscow, Russia

hardware means for computer simulation open the possibilities for well-founded and detailed forecast of the ecological situation with a reliability determined only by the completeness and consistency of the initial data. Such data are collected with the help of mobile and airborne lidar measuring systems installed terrestrially, aerially or in space [2 – 6]. The current progress in computer technologies and development of the latest software techniques and hardware for monitoring large bodies of data allow online ecological monitoring at a highly advanced level.

2. Structure of multiwave mobile lidar complexes

Three mobile lidar complexes (MLCs) whose photographs are shown in Fig. 13 in Ref. [7] were developed at the Laser Systems Ltd in 2003 – 2004. These complexes are currently operating in various climatic zones of Russia (central zone, desert and wet subtropics) and are used for remote laser sounding of atmosphere in the wavelength range from near ultraviolet (266 nm) to far infrared (11 μm). The MLC's sounding range of the atmosphere is 15 km.

Figure 1 shows the structural diagram of an MLC (see Section 10 for details). All the main channels of the MLC provide the same probing range. High backscattering coefficients of the atmosphere in the short-wavelength (visible and near-IR) range allow the detection of lidar signals at a distance of about 15 km using the traditional methods of direct detection of the backscattered radiation. As for the far-IR range (9 – 11 μm), probing of the atmosphere at such distances can be performed only by a heterodyne lidar with a large receiving aperture.

The use of a heterodyne lidar in the regime of coherent detection of scattered radiation for measuring the wind velocity and the absorption coefficient of the atmosphere required the development of schemes combining the possibilities of a coherent lidar and a differential absorption lidar. Moreover, it was also necessary to build a tunable two-channel single-frequency pulsed CO_2 laser system generating probe pulses at any of the 60 lines of the vibration – rotation spectrum of CO_2 and suitable for using on vehicles.

To perform a rapid and complex analysis of the ecological situation, synchronised data on aerosol and gas components of the atmosphere are required because the characteristic lidar probing times may be comparable with the times of variation of the atmosphere itself. Therefore, it is necessary to develop systems combining a simultaneous and independent operation of the solid-state lasers of an aerosol lidar and CO_2 lasers of a differential absorption heterodyne lidar. Moreover, the radiation scat-
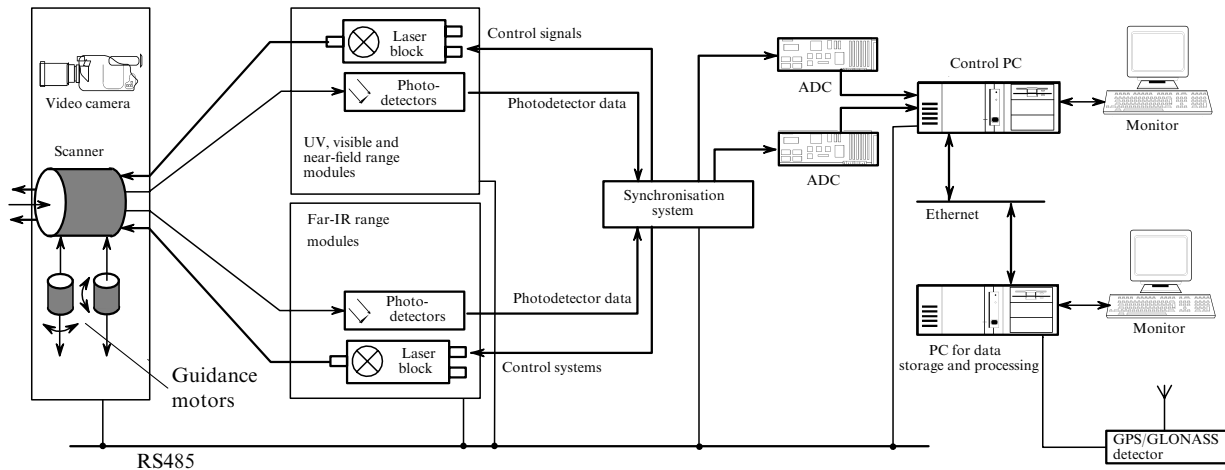
Figure 1. Structural diagram of an MLC.

tered by atmosphere and collected by a receiving telescope should be analysed simultaneously in the short-wavelength and long-wavelength ranges. This problem was solved by designing a transmitter–receiver telescope providing simultaneous operation of all MLC channels in the wavelength range from 266 nm to 11 μm.

The aerosol lidar in the MLC also detects the atmospheric aerosol, determines its concentration and analyses its physical origin. For this purpose, an aerosol Mie-lidar, a polarisation lidar, and a fluorescence lidar are combined into a single functional unit. Therefore, the data on the aggregate state of aerosol particles and their shape provided by the polarisation lidar are synchronised with the data on the chemical composition of the aerosol particles obtained from the fluorescence lidar, as well as with the measured concentration of the aerosol particles.

The surrounding space is scanned by a multiwave single-mirror or two-mirror scanner, which is common for all the channels and provides a continuous combining of the fields of view of all lidar channels irrespective of the current direction of probing. Such a complex approach was realised in the optical scheme of the MLC. Figure 2 shows the arrangement of the inner parts of the MLC. Table 1 presents the basic parameters of the MLC.

Table 2 shows the difference in the designs of mobile lidar complexes used for solving various problems. For example, MLC-1 and MLC-3 are equipped with single-mirror scanners allowing track investigations for angles not exceeding 20° to the horizontal. MLC-2 is equipped with a

double mirror scanner and allows probing of the entire upper hemisphere.

Table 1. Basic parameters of the MLC.

Minimum detection range	0.5 km
Maximum detection range[*]:	
for aerosol channel	up to 15 km
IR channel	up to 15 km
for UV channel	up to 5 km
Resolving power	200 m
Detectable gas impurities	
CO_2 DAS channel	hydrocarbons, freons, organophosphates, etc.
Ti : sapphire DAS channel	SO_2, NO_2, O_3, Cl_2, etc.
Nd : YAG channel	aerosol
Observation angles	
Vertical direction (elevation)	$-7 ... +15°$
Horizontal direction (azimuth)	$\pm180°$
Minimum scanning step	$40''$
Maximum angular velocity of scanner	$8°\ s^{-1}$
Tuning range	
CO_2 TEA (heterodyne)	$9-11$ μm
Nd : YAG (SHG, THG, FHG)	1064 nm (532, 355, 266 nm)
Ti : sapphire (SHG, THG)	$700-960$ nm $(350-480,$ $230-310$ nm)

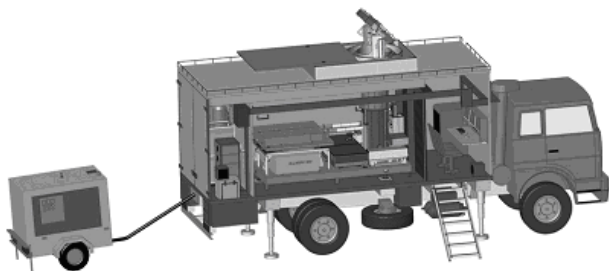Note: Depends on weather conditions and maximum visibility range.

Figure 2. Organisation of the inner space of an MLC (a container without the wall shows the optical slab with laser, optical and electronic equipment of the MLC, as well as the working place of the operator.

Table 2. Subsystems of mobile lidar complexes.

Subsystems	MLC-1	MLC-2	MLC-3
Scanner type	one-mirror	two-mirror	one-mirror
Tunable heterodyne CO_2 DAS	+	+	+
Doppler wind CO_2 lidar	+	+	+
Short-wavelength aerosol lidar (four Nd : YAG harmonics)	+	+	+
Short-wavelength DAS	+	+	
Fluorescence lidar			+
Polarisation lidar (fourth and second Nd : YAG harmonics)	+	+	
Turbulent lidar		+	

3. Multiwave transmitter – receiver telescope

The telescope in an MLC works in a broad spectral range and combines the functions of radiation receiving and transmission. It is assembled according to the Mersenne scheme and has an aspherical principal mirror with an optical diameter of 500 mm and a relative aperture of 1:2 (Fig. 3). The magnification of the telescope is $M = 7$. The secondary parabolic mirror has a drive mechanism, which allows focusing of the telescope in the range from 500 m to infinity.

In the long-wavelength range, the telescope is used for radiation transmission and reception. The area of its aperture is divided into transmitting and receiving zones (Fig. 3b) in contrast to [8, 9] in which the receiving and transmitting schemes are completely separated. The short-wavelength channels, operating in the direct detection mode, use the entire aperture area of the telescope for receiving backscattered radiation, while the probe radiation is trans-mitted through independent input mirrors. The telescope is fixed on a common optical plate (Fig. 3a) together with all the laser emitters, transport optics elements and receivers. The plate serves as the common base for all the optical elements, has a welded honeycomb structure and provides a high rigidity despite a comparatively small mass.

4. Scanning optics

The space is scanned with a common one- or two-mirror scanner, which changes simultaneously the position of the optical axes of all the receiving and transmitting channels. On the one hand, this allowed a stable mutual adjustment of all the MLC channels irrespective of the angular position of the probing line, and on the other required the development of a universal coating for the optical elements of the telescope and the scanner working in a broad wavelength range. This multilayer metal – dielectric coating deposited on a CO115M devitrified glass substrate provides the reflectivity no less than 0.95 in the wavelength range from 355 nm to 11 μm and no less than 0.87 at 266 nm.

The one-mirror scanner is retracted during travelling into the MLC container with the help of a special drive mechanism and is hermetically covered by a lid. The scanning range over the angle of elevation is between $-7°$ and $+20°$, while the azimuthal scanning range is $\pm180°$. The kinematic scheme of the two-mirror scanner allows a probing of the entire upper hemisphere. The drive for rotating the scanning mirrors is based on direct-drive dc torque engines. The precision and repeatability of the angular position of the probing line are determined by the class of the angle-data transmitter and are $40''$. Video observation is performed synchronously with lidar probing with the help of a digital video camera with a variable focal length in the visible spectral range and a television set with a bolometric focal array in the far-IR region.

All large-size mirrors of the telescope and the scanner were made of a devitrified glass and fastened with a relief providing the preservation of the optical quality of the surface in all operational modes and for all orientations of the mirrors.

5. Optical scheme of the MLC

The optical schemes of the MLC components are shown in Figs 4 – 7. The MLC contains the following subsystems.

(1) A Nd : YAG laser-based aerosol lidar for the visible and near-IR ranges. The laser operates on any of the four harmonics (266 – 1064 nm) with a pulse repetition rate of 10 – 25 Hz. The pulse energy at the fundamental harmonic is 600 mJ. Radiation is detected with photomultipliers (266 – 532 nm) and an avalanche photodiode (1064 nm).

(2) A short-wavelength differential absorption and scattering (SW DAS) lidar, which is mainly used for measuring the concentration of oxides of nitrogen and sulphur, and any other gases whose absorption spectra display contrast features in the wavelength ranges 700 – 960 nm, 350 – 480 nm and 230 – 310 nm.

(3) A long-wavelength differential absorption and scat-tering (LW DAS) heterodyne CO_2 lidar, which is mainly used for measuring the concentration of high-molecular substances.

(4) A coherent Doppler wind lidar constructed with the same elemental base as an LW DAS lidar. The only difference between these two types of lidars lies in the
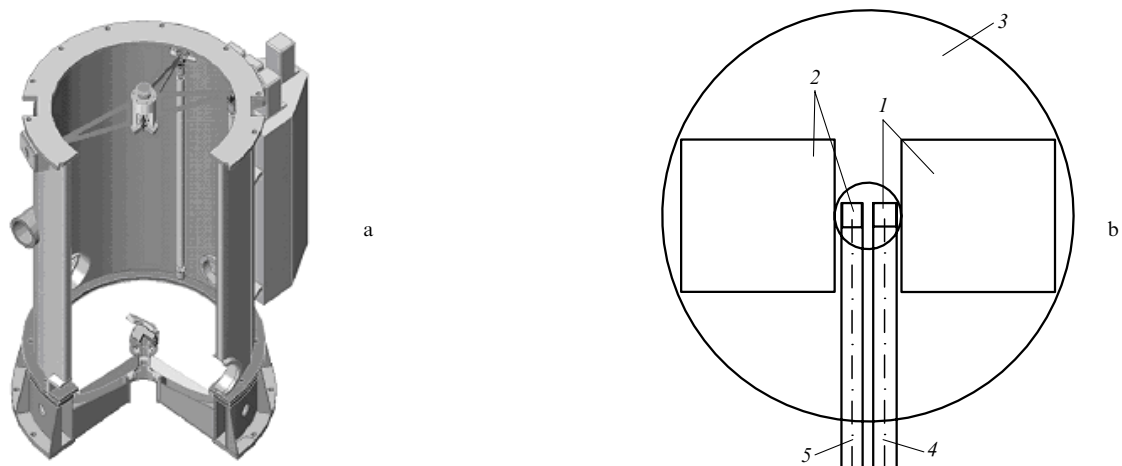
Figure 3. (a) Sectional view of the transmitter – receiver telescope, and (b) arrangement of receiving and transmitting long-wavelength channels at telescope mirrors: (*1*) region of radiation extraction; (*2*) region of radiation reception; (*3*) principal mirror; (*4*) output probe beam; (*5*) radiation being received.
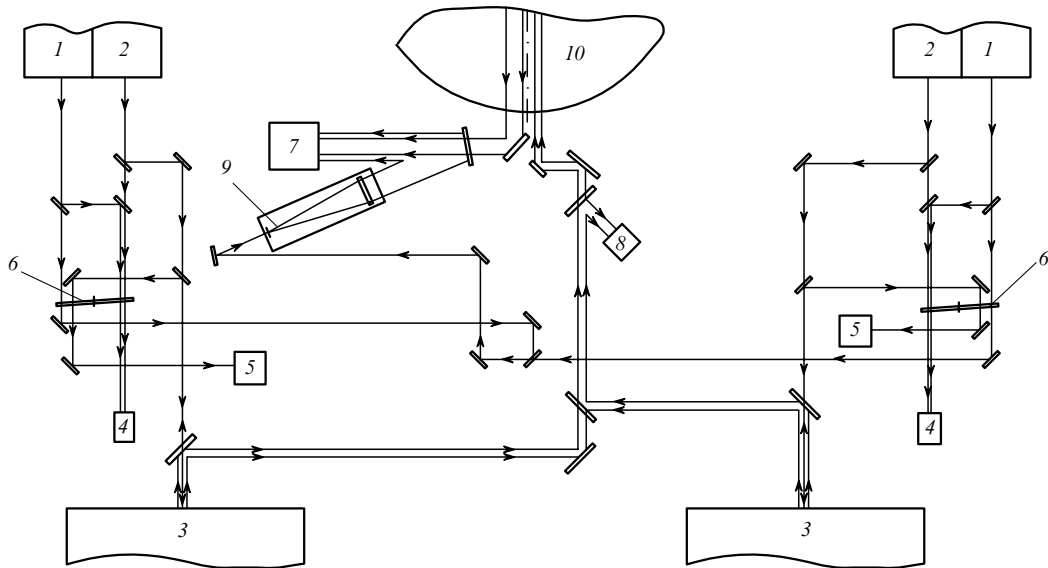
Figure 4. Scheme of the long-wavelength heterodyne channel: (*1*) heterodyne laser; (*2*) injector laser; (*3*) TEA laser; (*4*) cooled broadband detector of the '20 MHz' system; (*5*) pyroelectric detector of the AFT system for the TEA laser cavity; (*6*) shutter; (*7*) 25-element cooled MCT array detector; (*8*) detector of the synchronisation system; (*9*) telescopic heterodyne beam expander; (*10*) transmitter – receiver telescope.
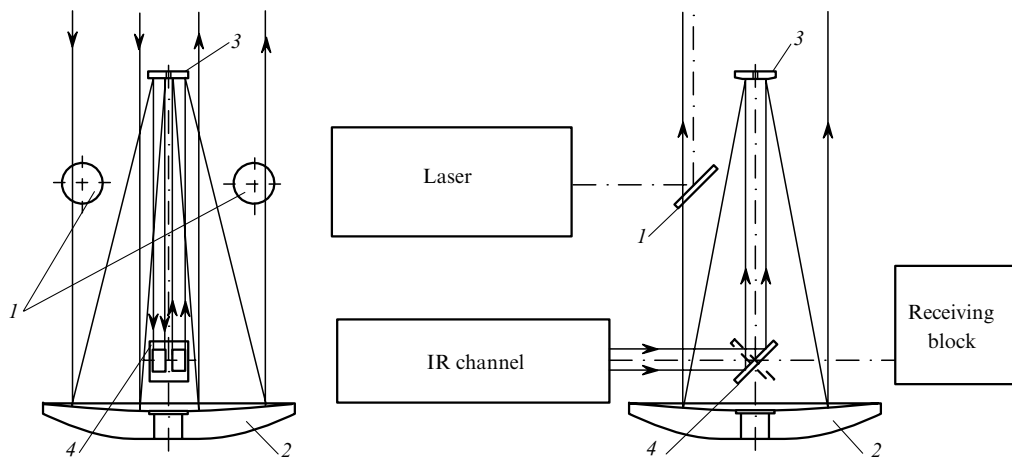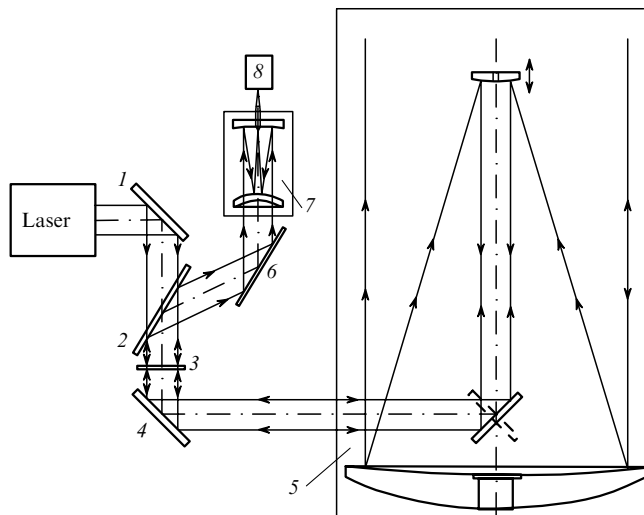

Figure 5. Scheme of the transmitter – receiver telescope: (*1*) output mirrors of the short-wavelength channel; (*2*) principal mirror of the telescope; (*3*) secondary mirror; (*4*) output beamsplitter.

technique of signal processing. The wind velocity in the range up to 20 m s^{-1} can be determined by measuring the Doppler shift of the scattered radiation frequency.

(5) A turbulent lidar operating at a wavelength of 532 nm for measuring the height profile of the structural constant of the atmospheric turbulence. The operation of this lidar is based on the measurement of the focal spot size. The 532-nm second-harmonic pulses from a Nd : YAG laser are used as the probe radiation. The transmitter – receiver telescope is focused at a certain distance. The radiation scattered from the waist region forms an image at the focus of the forming system of the turbulent lidar. The parameters of this image contain information about the overall effect of atmospheric turbulence on the path interval from the transmitter – receiver telescope to the focal point. After a series of measurements made on several horizontal and inclined paths, the vertical profile of the structural constant of atmospheric turbulence C_n^2 is reconstructed by mathematical data processing.

In the turbulence measurement regime (Fig. 6), the 532-nm second-harmonic radiation of a Nd : YAG laser is directed to the receiving and transmitting unit. The laser pulse reflected from mirror (*1*) passes through Brewster plate (*2*) and quarter-wave plate (*3*) from where it is directed by mirror (*4*) to transmitter – receiver telescope (*5*) with focusing properties. The backscattered radiation from the atmosphere passes once again through the quarter-wave plate and changes its polarisation to orthogonal relative to the initial polarisation, which allows the radiation to be reflected from the Brewster plate. The scattered signal is directed by mirror (*6*) to Maksutov – Cassegrain objective (*7*) which focuses it to unit (*8*) for measuring the focal spot diameter.

(6) A fluorescence lidar for determining the nature of the atmospheric aerosol from the fluorescence spectrum. Fluorescence is excited by the 266-nm laser pulses. The fluorescence spectrum is recorded in the wavelength range 300 – 500 nm with a grating monochromator equipped with a 32-element photomultiplier.

Figure 6. Turbulence measurement scheme: (*1*, *4*, *6*) mirrors; (*2*) Brewster plate with a dielectric coating; (*3*) quarter-wave plate; (*5*) transmitter – receiver telescope; (*7*) Maksutov – Cassegrain objective; (*8*) unit for measuring the focal-spot size

(7) A polarisation lidar used for determining the physical characteristics (size, state of aggregation) of aerosol particles. The 532-nm second-harmonic radiation from a Nd : YAG laser is used for probing. The backscattered radiation from the atmosphere is split by mirror (*1*) (Fig. 7) with a dielectric coating, which reflects visible radiation and transmits near-IR radiation. Feld stops (*3*) are located in the common focal planes of lenses (*2*) and (*4*) for the visible and IR channels. Replaceable optical filters and beamsplitter (*5*) are mounted on a revolving
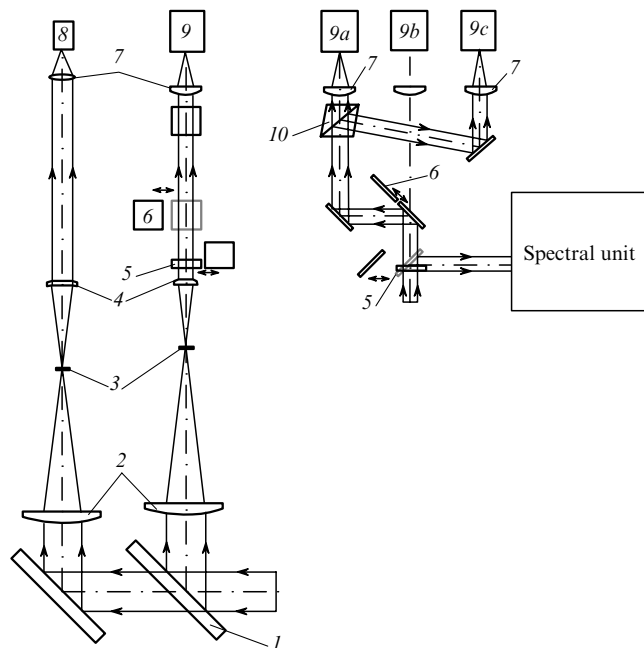
Figure 7. Scheme of the receiving block of the shot-wavelength channel: (*1*) mirror with a dielectric coating; (*2*, *4*) objective lens system; (*3*) diaphragms; (*5*) replaceable optical filters and deflecting mirror on a revolving turret; (*6*) mobile mirror; (*7*) focusing lenses; (*8*) avalanche photodiode; (*9*) photomultiplier; (*10*) Glan – Taylor prism.

turret and are used for narrowing the spectral range and for fluorescence analysis, respectively. In the latter case, a mirror is introduced into the beam and a part of radiation is directed to a monochromator for studying the fluorescence spectrum. In the absence of mirror (*6*), the complex works as an aerosol lidar or a SW DAS lidar. The scattered radiation is focused by lens (*7*) on photomultiplier (*9b*). Mirror (*6*) is introduced into the beam in the polarisation lidar regime, a part of the radiation being directed to a Glan – Taylor prism, which splits the scattered radiation into components with orthogonal polarisations and directs them to photomultipliers (*9a*) and (*9c*). The near-IR radiation at 1064 nm is focused on an avalanche photodiode.

Table 3 presents the parameters of lasers used in the MLC. An important specific feature of the optical scheme of the long-wavelength heterodyne lidar is that the two-channel laser system operating in the differential absorption technique uses a CMT (cadmium – mercury – telluride) array detector. This provides identical characteristics for both channels. The operation of the channels was synchronised with the help of light choppers protecting the detectors from direct high-power TEA-laser pulses and commuting the radiation from two local oscillators.

Table 3. Parameters of lasers.

Neodymium laser (YAG : Nd^{3+})	
Pulse energy (mJ) at wavelengths	
1064 nm	$\geqslant 600$
532 nm	$\geqslant 400$
355 nm	$\geqslant 170$
266 nm	$\geqslant 90$
Pulse duration/ns	10 – 80
Pulse repetition rate/Hz	10 – 25
Ti : sapphire laser	
Pulse energy (mJ) at wavelengths	
700 – 900 nm	$\geqslant 70$
350 – 450 nm	$\geqslant 20$
230 – 300 nm	$\geqslant 10$
Pulse duration/ns	30 – 40
Pulse repetition rate /Hz	10
Two-channel single-frequency CO_2 laser system based on pulsed TEA lasers	
Pulse energy/mJ	
at 10P(20) line	$\geqslant 500$
at lines with indices 10 – 30	300 – 400
at branch edges	100 – 300
Wavelength range (number of CO_2 lines in vibration – rotation spectrum)	60
Pulse duration/μs	1 – 2
Pulse repetition rate/Hz	10

6. Single-frequency two-channel laser system of a heterodyne CO_2 lidar

A heterodyne CO_2 lidar consists of two synchronised channels with the same axis of vision but tuned to different wavelengths. The pulse repetition rate in each channel is 10 Hz and the time interval between the channels is 10 μs.

Each channel includes a tunable single-mode TEA laser and two tunable single-frequency waveguide lasers: an injector laser specifying the radiation frequency of the

TEA laser and a heterodyne laser specifying the single-frequency reference radiation on the receiving array. The lasers are tuned to the same line of the vibration – rotation spectrum. The system of automatic frequency control (AFC) by varying the resonator length with the help of piezoelectric ceramic drives tunes and maintains matched radiation frequencies of the lasers. The injector laser is tuned to the longitudinal mode with the maximum power, the longitudinal mode of the TEA laser cavity is tuned to the injector frequency, and the heterodyne radiation frequency is detuned by 20 MHz from the injector frequency. In the absence of injection, lasing in TEA lasers occurs at several longitudinal modes with characteristic interference beats (Fig. 8a). In the injection regime, the TEA laser generates single-frequency pulses with a spectral width of 1 MHz determined by the laser pulse duration (Fig. 8b). The wavelet analysis [10] of the lidar echo-signal with heterodyne reception from a topographic target (Fig. 9b) shows that the spectral width of reflected radiation is mainly determined by the broadening due to a limited duration of the laser pulse. Such a two-channel tunable heterodyne lidar system was realised for the first time on a vehicle.

7. Coherent CO_2 lidar

This lidar, which is one of the most important components of the MLC, has been developed on the basis of single-frequency TEA CO_2 lasers, cw single-frequency CO_2 lasers, and a broadband CMT array detector. The lasers provide tuning to any of the 60 lines of the vibration – rotation spectrum of CO_2 in the wavelength range from 9 to 11 μm. The cw CO_2 lasers – injector laser (2) and heterodyne laser (1) (see Fig. 4) are enclosed in a single casing. A part of the injector radiation reflected from the beamsplitter and highly reflecting mirror is directed to the cavity of TEA laser (3). The injector radiation reflected by the cavity is directed by the beamsplitter and mirror to detector (5), providing the operation of the AFC system. The rest of the injector radiation is mixed with the heterodyne radiation at the beamsplitter and falls on cooled broadband receiver (4) used to stabilise the intermediate heterodyne frequency. The heterodyne beam expanded by Galileo telescope (9) is mixed with the radiation scattered in the atmosphere at the beamsplitter and falls on broadband CMT array detector (7). A part of the TEA laser pulse energy incident on receiver (8) is used for triggering the synchronisation system and analogue-to-digital converter. Chopper (6) is used for synchronisation of the entire system and protection of receivers (4, 5) from the TEA laser pulse.

The probe pulse reflected from beamsplitter (4) (see Fig. 5) falls on transmitter – receiver telescope (3, 2) and is directed to the atmosphere. The backscattered radiation is collected by the same telescope and directed back to the IR channel where it is mixed with heterodyne radiation at the array detector.

Figure 10a shows the results of atmosphere probing in the long-wavelength heterodyne channel. The same figure also shows the curve of the current values of the mean-square deviation (MSD) for the high-frequency noise. The lidar signal approaches the noise level at a distance of 15 – 17 km.
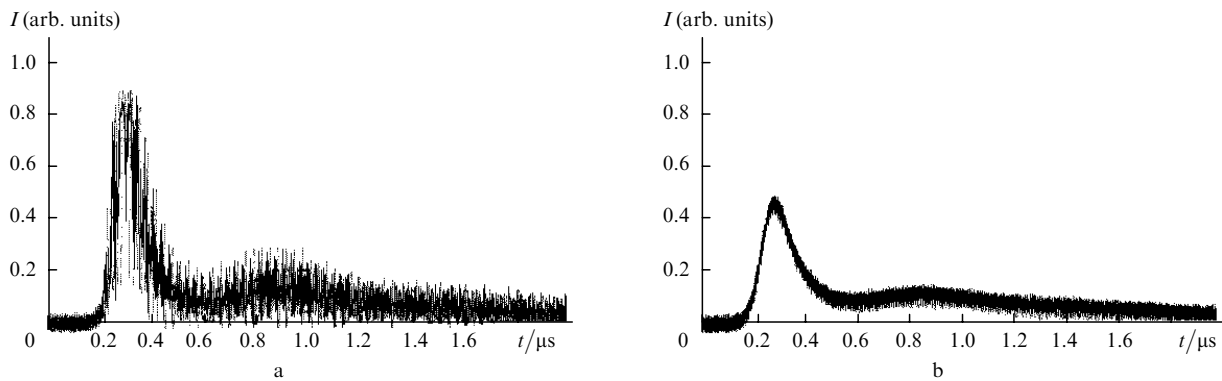

Figure 8. Shapes of TEA laser pulses [9R(18) line] in (a) free-running and (b) injection lasing regimes.
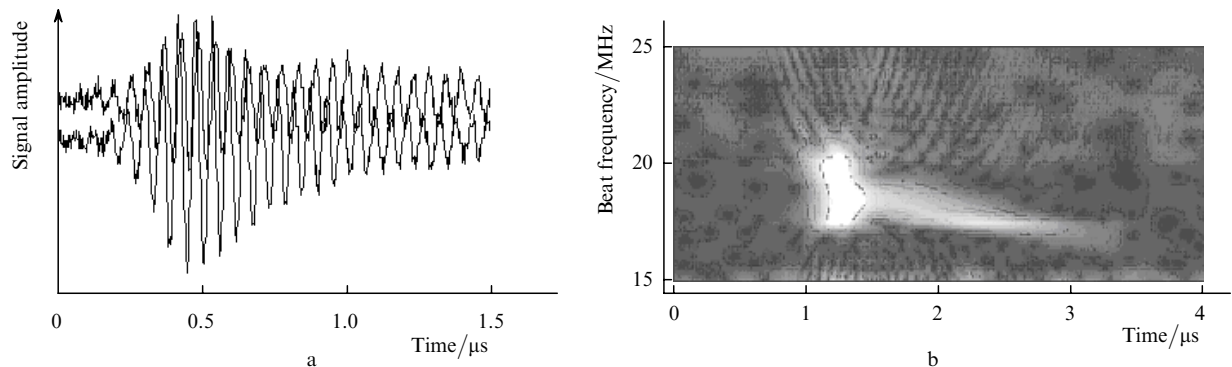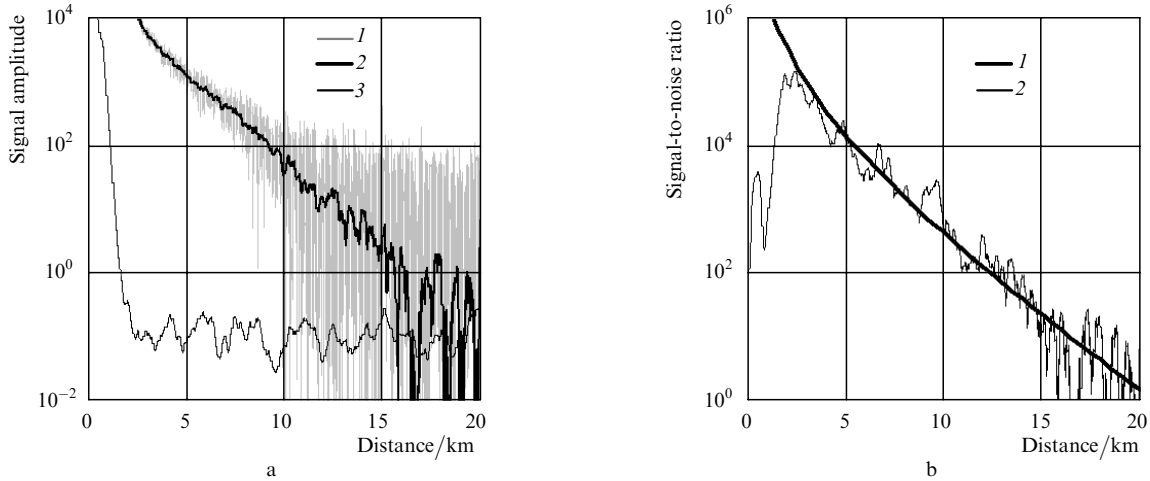

Figure 9. Long-wavelength heterodyne lidar signal reflected from a topographic target at a distance of about 3 km; (a) time sweep of signals from two different elements of the array detector (total duration 2 μs) (b) wavelet spectrum (total duration 4 μs, beat frequency range 15 – 25 MHz).

Figure 10. (a) Backscattered signal obtained in the heterodyne regime in far IR range [9R(30) line]: (*1*) lidar signal; (*2*) signal smoothed by the exponential filter; MSD of noise, and (b) estimates of the signal-to-noise ratio obtained by formulas (1) [curve (*1*)] and (3) [curve (*2*)].

Signal-to-noise ratio. The heterodyne detection of scattered radiation received with the help of a large receiving telescope considerably improves the signal-to-noise ratio (SNR) and the working range of the lidar system [11]. The required pulse energy and the attainable probing range is estimated from the relation [12]

$$\mathrm{SNR} = \frac{1}{2} \frac{E\beta(\pi)\lambda A \exp(-2\alpha R)}{hBR^2\{1 + (1 - R/F_d)^2 [\pi D_e^2/(4\lambda R)]^2 + (D/2r_c)^2\}}, \quad (1)$$

where $D_e = 0.61D$ is the equivalent diameter of the telescope aperture; D is the diameter of the receiving aperture; F_d is the focusing distance; A is the area of the receiving aperture; B is the width of the transmission band of the receiving system; E is the pulse energy; $\beta(\pi)$ is the volume backscattering coefficient; r_c is the coherence range; α is the extinction coefficient; and R is the detection range.

To estimate the SNR, it is sufficient to take into account that the signal oscillations whose time scale is smaller than the probe-pulse duration τ are nothing but noise. In the presence of a lidar signal obtained upon probing by a single pulse, the instantaneous root-mean-square value of the noise can be written in the form

$$N(t) = \left\{ \int_{-\infty}^{t} \left[S(\eta) - \int_{-\infty}^{\eta} S(\xi) \exp[-(\eta - \xi)/\tau]\mathrm{d}\xi \right]^2 \right.$$
$$\left. \times \exp[-(t - \eta)/\tau]\mathrm{d}\eta \right\}^{1/2}, \quad (2)$$

where $S(t)$ is the initial lidar signal. Filtration of the lidar signal over a time scale τ is performed with the help of an integral operator with an exponential core; in this way, the part of the signal not connected with the noise is separated. Then, the SNR can be calculated from the expression

$$\mathrm{SNR} = \int_{-\infty}^{t} S(\xi) \exp[-(t - \xi)/\tau]\mathrm{d}\xi \Big/ N(t), \quad (3)$$

Figure 10a shows the initial lidar signal obtained on the heterodyne receiver channel from a single probe pulse [curve (*1*), sampling frequency 50 MHz], the signal filtered with the scale $\tau \approx 2$ μs [curve (*2*)] and an estimate of the MSD noise obtained from expression (2) [curve (*3*)]. The experimental results (3) and the estimate obtained by using formula (1) are presented in Fig. 10b. The width B of the transmission band of the receiving system is assumed to be 16 MHz. At a distance of about 15 km, both estimates of the SNR approach unity. Estimates show that at limiting distances, SNR decreases by a factor of about ten for $\Delta R \approx$ 5 km; hence, an accumulation of data for about 10 s increases the range by 5 km for a pulse repetition rate $f = 10$ Hz.

Effect of turbulence on the operation of a heterodyne CO_2 lidar. The atmospheric turbulence, which violates the spatial coherence of the scattered radiation, may influence the efficiency of heterodyne reception in a number of cases. The extent and the nature of its influence are determined by the relation between the coherence range $r_c = 1.46(k^2 C_n^2 R)^{-3/5}$ and the diameter $d_0 = D/N^{1/2}$ of the receiving objective per element of the receiver (N is the number of elements in the multielement receiver).

Three typical cases are considered:

(1) $d_0 \ll r_c$. In this case, an equiphase signal arrives at each receiver element from the atmosphere, and the atmospheric turbulence weakly affects the heterodyne reception efficiency.

(2) $d_0 \approx r_c$. In this case, a random-phase signal arrives at each element of the receiver. This situation is illustrated in Fig. 9a showing the time sweep of two synchronous signals obtained from two different elements of the array detector. The phase difference of the signals depends on the detection range and varies from experiment to experiment.

(3) $d_0 \gg r_c$. The variable component of the signal at each receiver tends to zero with decreasing r_c.

The criterion determining the working range of the heterodyne receiver channel has the form

$$\frac{r_c}{d_0} = \frac{1.46(k^2 C_n^2 R)^{-3/5}}{D} \sqrt{N} > 1, \quad (4)$$

where k is the wave number and C_n^2 is the structural constant of atmospheric turbulence.

An analysis of the statistics of turbulence parameters [13] shows that the above condition is satisfied for all practically important cases of application of mobile lidar complexes.

7.1 Coherent Doppler wind lidar

When a coherent CO_2 lidar is used for measuring the wind velocity, it functions as a Doppler lidar. In this case, the single-frequency CO_2 laser system may operate on either channel and on any of the lines of vibration–rotation spectrum of CO_2. The unit for processing of signals from the heterodyne array receiver gives an intermediate frequency signal (20 ± 8 MHz) formed due to interference of the scattered radiation received from the atmosphere and the radiation emitted by the local oscillator. The scattered radiation has a Doppler frequency shift proportional to the projection of the wind velocity on the direction of the probing path. The Doppler frequency shift for the 10-μm probe radiation is ~ 200 kHz m^{-1} s^{-1}.

The signal is digitised with a sampling frequency of 100 MHz. The duration of temporal realisation stored in the computer memory for each probe pulse and is 100 μs. Each pulse is processed after recording with the help of a digital fast Fourier transform (FFT) window filter. The width of the time window is determined by the desired accuracy of wind velocity measurement. As the window width is increased, the measurement accuracy increases but the spatial resolution deteriorates. The standard algorithm provides an accuracy of 1 m s^{-1} which corresponds to the smallest possible width $\tau_w = 5$ μs of the time window. In this case, the spatial resolution is found to be $c\tau/2 = 750$ m. The algorithm is adjusted flexibly and the required spatial resolution and precision of wind velocity measurements are selected in accordance with the problem being solved.

Figure 11a shows an example of the window Fourier analysis of the data obtained with a Doppler wind lidar. The experimental data were obtained by probing the horizontal atmospheric path. The temporal window of width $\tau_w \approx 5$ μs is displaced along the abscissa axis, the amplitude of the intermediate signal frequency is normalised, and the auto-correlation function and its Fourier transform are calculated. In this way, we obtain the normalised energy spectrum of a fragment of the lidar signal. This spectrum is plotted along a line parallel to the ordinate axis. The position of this line on the abscissa axis corresponds to the centre of the temporal window. Figure 11a shows a maximum at 21 MHz, corresponding to a wind velocity $(21 - 20) \times 10^6$ Hz$/200 \times 10^3$ Hz m^{-1} s $= 5$ m s^{-1}. The signal spectrum broadens with increasing distance, which is probably caused by the effect of atmospheric turbulence.

Figure 11b shows the distribution of the axial projection of the wind velocity along the probe path, reconstructed by the method of the window Fourier transform. The magnitude and sign of the Doppler frequency shift for the scattered radiation determine the magnitude and sign of the wind velocity projection on the direction of the probe path. The altitude profile of the wind velocity vector is measured by performing three successive measurements along three mutually perpendicular inclined paths. Subsequent processing makes it possible to calculate the altitude dependence of the horizontal and vertical components of the wind velocity from the measured values of the projections.

7.2 Coherent differential absorption CO_2 lidar

In a differential absorption lidar, two coherent CO_2 channels operate successively with a time interval of 10 ms and a pulse-pair repetition rate of 10 Hz. The working lines of the vibration–rotation spectrum are
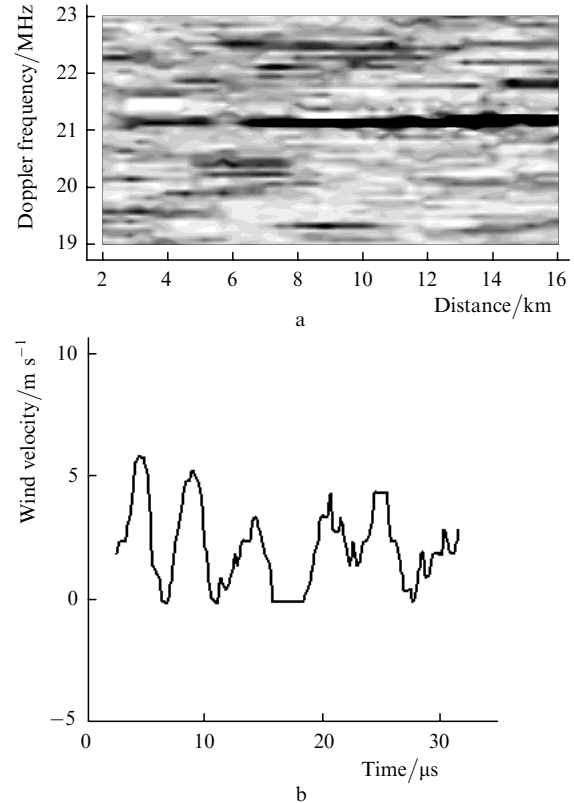
Figure 11. Results of wind velocity measurement along an inclined path at an angle of $10°$ to the horizontal: (a) data of wind Fourier analysis of the signal from a Doppler wind lidar; (b) distribution of the axial projection of the wind velocity.

established beforehand, depending on the substance whose concentration is to be measured. The choice and alignment of the appropriate position of the diffraction gratings are made automatically. Figure 10a shows an example of a single lidar signal. The concentration C of the substance is calculated by differentiating the results of measurements [1]:

$$C = \frac{1}{2\Delta\sigma} \frac{d}{dR} \ln \frac{I_{on}}{I_{off}}, \qquad (5)$$

where $\Delta\sigma$ is the differential absorption cross section ($\Delta\sigma = \sigma_{on} - \sigma_{off}$), and I_{on} and I_{off} are the lidar signals obtained at different wavelengths. Such an operation without preliminary measures leads to a considerable enhancement of the effect of noise, which renders lidar measurements impossible even at distances where the SNR (1), (3) is much larger than unity for the initial lidar signals. This problem is solved by post-processing of the signal, which involves a lowering of the noise level at the expense of spatial resolution.

The spectral resolution of a differential absorption heterodyne CO_2 lidar is limited by a finite duration of the probe laser pulse and a specified error of the concentration measurement. By passing to finite differences in (5), we can easily obtain a relation between the spatial resolution ΔR, the minimum concentration C_{min} of the absorbing impurity, the differential absorption cross section $\Delta\sigma$ and the SNR for the initial lidar signal:

$$\Delta\sigma C_{min} \, \text{SNR} \, \Delta R \geqslant A_c, \qquad (6)$$

where A_c is a constant of the order of unity. Therefore, the sensitivity of the lidar for the best special resolution can be written in the form:

$$C_{\min} = \frac{A_c}{\Delta\sigma \, \text{SNR} \, c\tau}. \qquad (7)$$

For example, the differential absorption cross section of ammonia for λ_{on} [10R(12) line] and λ_{off} [9R(30) line] is $\Delta\sigma = 55.8 \text{ atm}^{-1} \text{ cm}^{-1}$. For the same values of SNR that are obtained in the receiver channel of the MLC (see Fig. 10b) and spatial resolution limited only by the pulse duration, the minimum detectable concentration of ammonia at the limiting distance of 15 km is ~ 1 ppm, which nearly corresponds to the smell sensitivity.

The choice of laser lines for sounding a substance is made on the basis of a meticulous analysis of the required range, sensitivity and possible impurities that can distort the absorption spectrum of the medium under study. The minimum detectable concentrations of some substances for limiting ranges for the 10R(12) and 9R(30) lines are presented in Table 4. At shorter ranges, the sensitivity increases in accordance with the increase in the SNR (see Fig. 10b). In any case, the threshold concentration is inversely proportional to the differential absorption cross section and depends on the choice of the wavelengths of the probe radiation.

Table 4. Differential absorption cross section and lidar sensitivity for some gases [λ_{on} – 10R(12) line, λ_{off} – 9R(30) line].

Molecule	$\sigma_{\text{on}}/$ atm^{-1} cm^{-1}	$\sigma_{\text{off}}/$ atm^{-1} cm^{-1}	$\Delta\sigma/$ atm^{-1} cm^{-1}	$C_{\min}/$ppm
COF_2	4.1	0	4.1	20.3
C_2H_4	2.1	0	2.1	39.7
C_2H_3Cl	1	0.1	0.9	92.6
NH_3	56	0.2	55.8	1.5
$CClO_3$	6.8	0.25	6.55	12.7
C_2H_5OH	6.5	1.95	4.55	18.3
CCl_2F_2	1.32	0	1.32	63.1

If the size of the contamination region is smaller than the spatial resolution of the lidar, the product $(Cc\tau)_{\min}$ of concentration and the size of the region along the probe path can be treated as the parameter determining the sensitivity of the system. A point-to-point calibration of the differential absorption CO_2 lidar is carried out by the cell method for NH_3 ($\lambda_{\text{on}} = 10.716 \text{ μm}$ [10P(34)], $\lambda_{\text{off}} = 10.588 \text{ μm}$ [10P(20)]) and SF_6 ($\lambda_{\text{on}} = 10.549 \text{ μm}$ [10P(16)], $\lambda_{\text{off}} = 10.492 \text{ μm}$ [10P(12)]).

8. Short-wavelength aerosol lidar

Figure 12 shows the preliminary characteristic results of sounding of the natural atmospheric aerosol by a short-wavelength aerosol lidar. The structure of the aerosol layer at a distance of $8 - 13$ km can be seen clearly. The reduced signal was obtained without accumulation at the wavelength 532 nm, the SNR approaching unity at a distance of about 15 km. The photomultiplier gating which cuts off scattered radiation (arriving from a distance of up to 6 km in the present case), makes it possible to operate with the maximum gain and, hence, the maximum range. The minimum sounding range is ~ 500 m.
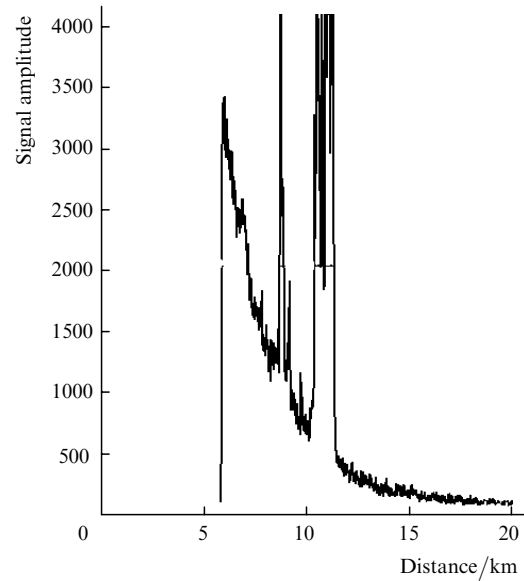
Figure 12. Lidar signal obtained without accumulation during probing of the cloud layer along an inclined path at a wavelength of 532 nm.

The atmospheric aerosol can be probed by any of the four harmonics of the Nd : YAG laser (1064, 532, 355 and 266 nm). The short-wavelength laser module has two independent channels (see Fig. 4) and a technical possibility of choosing any pair of wavelengths (1064 and 532 nm, 1064 and 266 nm, 355 and 532 nm, 355 and 266 nm) exists for the two-wave probing regime. This wavelength set allows us to probe almost any natural atmospheric aerosol and to determine its concentration and the effective size of the particles.

9. Short-wavelength differential absorption and scattering lidar

An SW DAS lidar is based on a two-channel tunable Ti : sapphire laser pumped by the second harmonic of a Nd : YAG laser (the laser parameters are given in Table 3). The laser emits in the spectral regions $700 - 900$ nm, $350 - 450$ nm, and $230 - 300$ nm, allowing the measurement of concentrations of various ecological pollutants (NO_2, SO_2, etc.) and other substances having absorption bands in the emission range of the Ti : sapphire laser. Scattered radiation is received by the entire aperture of a transmitter – receiver telescope and is focused on a photomultiplier.

Equation (6) is valid for the basic parameters of the SW DAS lidar (as well as for the parameters of the LW DAS lidar). A specific features of the short-wavelength lidar is that a small pulse duration ($30 - 40$ ns) allows a further increase in the sensitivity by lowering the spatial resolution ΔR to values which are provided by the CO_2 system and the MLC as a whole. Therefore, the sensitivity of the SW DAS lidar can be calculated from expression (6) in which $c\tau$ should be replaced by ΔR, which is higher than $c\tau$. The concentration of NO_2 was measured at the wavelengths $\lambda_{\text{on}} = 448.5$ nm and $\lambda_{\text{off}} = 446.9$ nm ($\Delta\sigma = 5.5 \text{ atm}^{-1} \text{ cm}^{-1}$).

The accumulation of data from several probe pulses increases the sensitivity by a factor of $(fT)^{1/2}$ due to an increase in the SNR, where T is the averaging time, which should not exceed the characteristic time of variation of the contamination being investigated. In actual practice, only
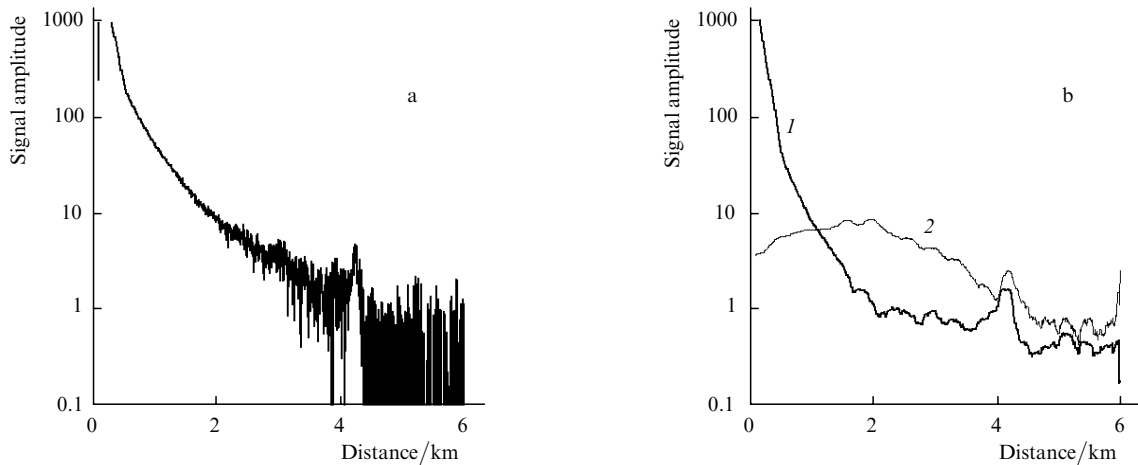
Figure 13. (a) Lidar signal obtained at a wavelength $\lambda_{on} = 448.5$ nm and (b) MSD of noise [curve (*1*)] and signal-to-noise ratio [curve (*2*)].

the results obtained by averaging over a considerably long time are reliable because individual lidar signals fluctuate sharply due to a change in the atmospheric conditions. Thus, when the results are averaged over 5 s for $f = 10$ Hz and $\Delta R = 200$ m, the short-wavelength lidar provides the detection of NO$_2$ at the concentration $C_{min} \approx 1$ ppm at limiting distances where the SNR ≈ 1. Figure 13 shows a characteristic lidar signal and the SNR. The SW DAS lidar was calibrated by the cell method by NO$_2$ ($\lambda_{on} = 448.5$ nm, $\lambda_{off} = 446.9$ nm) and SO$_2$ ($\lambda_{on} = 300.1$ nm, $\lambda_{off} = 299.5$ nm).

10. MLC control system

All the subsystems of the complex (see Fig. 2) form a single structure since they are combined into the aboard network through a commercial RS-485 interface. Each device in the complex connected to the network has its unique address. The exchange of information is initiated by the control computer in the batch regime, and the control is performed by the computer at the first work location WL1. The data from systems in the complex are supplied to an analogue-to-digital converter (with the sampling frequency from 20 to 100 MHz depending on the operating regime) after preliminary commutation in the synchronisation system. The signals are processes in real time, and the results are displayed on the WL1 screen, from where they are transferred to the visualisation and mapping system in the WL2. All the results of probing are stored in the data base. The WL1 and WL2 computers are connected through Ethernet.

The operation of transmitting and receiving devices as well as the data collection system is synchronised by means of a special synchronisation system via commands transmitted through the aboard network of the complex.

The control system provides a choice of the required operating regimes of the lasers, switches and attenuators of lidar channels, as well as the total synchronisation of all these systems. The scanning system provides a programmable rotation of the scanner mirror, while the data collection and processing system performs the measurement and accumulation of signals, the calculation of volume distributions and their positioning, and displays the results on the monitor screen.

In the sector scanning regime, the object is either specified according to target designation or identified in the panoramic scanning and video surveillance regime. The three-dimensional sector scanning is performed to estimate the emission intensity. In this case, the integrated values of the optical density are determined in each direction of the emission region.

Panoramic scanning involves a periodic study of the atmosphere (circular or sector lidar scanning) in the region of the object under control. The concentrations of the pollutants characterising the object under study are measured by aerosol probing and probing over differential absorption channels. This gives a set of 'lidarograms' for subsequent processing (statistics, growth dynamics, characteristic lifetimes, change in the concentration of pollutants, etc.)

Such an operating regime of the lidar complex requires real-time processing of a large body of data. Obviously, the overall information traffic can be estimated from the expression

$$S = N_c f \Delta \tau F B, \qquad (8)$$

where N_c is the number of simultaneously operating lidar channels; $\Delta\tau$ is the duration of a lidar signal; F is the sampling frequency; and B is the number of bits in a data word. In our case, the following parameters are typical: $N_c = 4$ (aerosol lidar, two differential absorption channels, and the fluorescence channel), $\Delta\tau = 100$ μs, $F = 50$ MHz, and $B = 16$. In this case, the data traffic is estimated at 3.2 Mbyte s^{-1}.

An express analysis of the lidar signals obtained in the sector scanning regime allows one to obtain the images of aerosol clouds superimposed on the map of the area. Visualisation of the motion of aerosols allows a prognosis of their propagation. The MLC operator receives all the necessary data for decision making, including the current cloud position, the aerosol concentration (depicted in the form of isolines directly on the map), the wind direction and velocity, and the concentration and cloud position being predicted.

11. Typical results of measurements

Figure 14 shows the results of measurements of the background concentrations of ammonia in a natural urban landscape. The concentration distribution map is
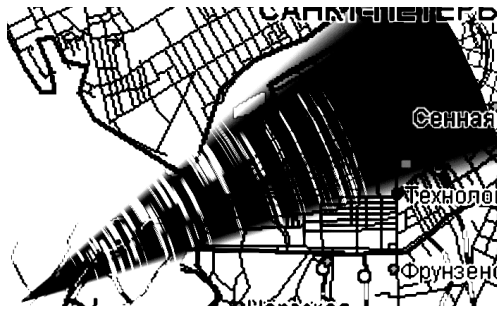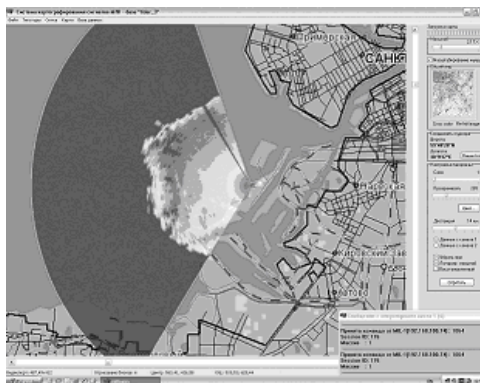
Figure 14. Results of measurement of the ammonia concentration in a natural urban landscape of St. Petersburg. The light regions in the probe sector correspond to areas with a concentration exceeding 1 ppm.

Figure 16. Results of measurement of the background concentrations of NO₂ in a natural urban landscape of St. Petersburg. The light regions in the probe sector correspond to areas with a concentration exceeding 1 ppm.

locked to the geographical coordinates with the help of a GPS receiver and is displayed on the WL2 monitor screen. Information for 100 pulse pairs is accumulated along each scanning direction. The amount of the data being accumulated and the scanning time for the sector are selected by the operator according to the requirements to the speed and accuracy of measurements.

Figure 15 shows the results of probing of natural atmospheric aerosol in the sector scanning regime at a wavelength of 1064 nm. The angle characterising the location during probing of the sector was constant (10°). The cloud layer terminates at a distance of 3–4 km, which corresponds to the upper boundary of 600–700 m of cloudiness. For a correct choice of the wavelength, a qualitative pattern of aerosol distribution and its real-time dynamics can be obtained by a periodically repeated probing of the sector in the single-wavelength regime, which provides the initial data for a short-term prognosis of aerosol propagation.

Figure 16 shows a map of the NO₂ concentrations measured under urban conditions with the short-wavelength differential absorption lidar on paths inclined to the horizon at an angle of 10°. Regularly repeating concentration maxima can be attributed to certain objects on the map of the city.

The results of measurements shown in Figs 14–16 were obtained between 12 noon and 5 pm on a cloudy summer day in July 2004. The lidar complex was located at a

position on the south-west of St. Petersburg over the shore of the Gulf of Finland. One can see from the figures that both western (sea) and eastern (land) sectors were chosen for probing

Figure 17 shows the results of remote lidar measurements of the spectrum of laser-induced fluorescence of protein (artificially prepared aerosol of albumin solution). The aerosol cloud was produced by a special aerosol generator by pneumatic spaying of the solution. The size of the cloud along the probing path was several metres. Excitation was performed by 266-nm laser pulses. Measurements were carried out under field conditions at night at a distance of about 1 km. A sample averaging over 200 pulses was performed by a method taking into account the statistical nature of the fluorescent signal, followed by the subtraction of the background fluorescence spectrum. The characteristic shape of the spectrum allows a detection of protein in the investigated aerosol from radiation emitted in the wavelength range 350–400 nm and 450–500 nm. Because of a strong solar illumination at daytime, measurements were performed in the spectral region below 400 nm. However, according to the conditions of the problem under study, such measurements should be made mainly at night.

Figure 18 shows the results of measurements of the vertical profile of the structural constant C_n^2 of atmospheric turbulence. Depending on the desired accuracy and the region of altitudes, the series of measurements of C_n^2 and data processing were performed during 10–15 minutes.

Figure 15. Distribution of atmospheric aerosol locked to the area, as seen on the monitor of the operator during probing of the sector in the aerosol lidar mode.
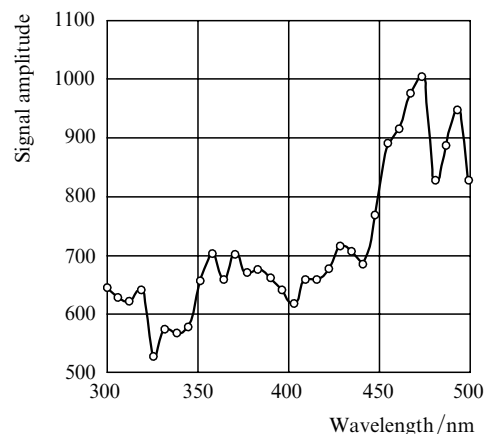

Figure 17. Spectrum of the laser-induced fluorescence in the aerosol of an aqueous solution of albumin, measured with the help of the fluorescent channel of the MLC.
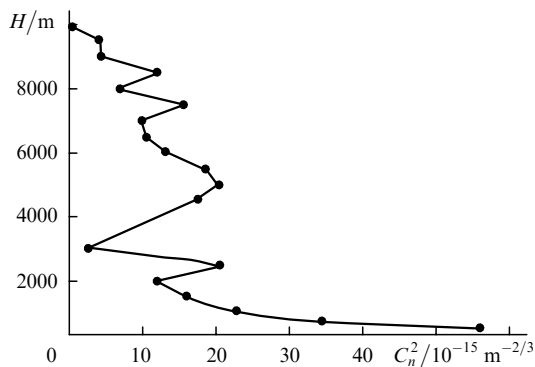
Figure 18. Altitude profile of the atmospheric turbulence structural constant C_n^2.

12. Conclusions

Thus, multiwave mobile lidar complexes (MLCs) have been designed and developed at Laser Systems Ltd. Three versions of vehicle-based MLCs have been realised. The entire body of the data on complex lidar probing obtained with the help of MLCs has been synchronised in space and time, covers a large area (the range of an MLC is 15 km), and is based on a unified methodological platform. The results of probing contain information on the concentration and physical nature of atmospheric aerosol, chemical composition of the gaseous phase of the atmosphere, wind and turbulence. The obtained data form the basis for a complex analysis of the ecological situation and prognosis of its development.

References

1. Measures R.M. *Laser Remote Sensing: Fundamentals and Applications* (New York: Wiley, 1984; Moscow: Mir, 1987).
2. http://www.nppgamma.com/lidar.htm.
3. *Samolet-laboratoria Optik-E* (*Flight Laboratory Optik-E*); http://www.iao.ru/ru/resources/equip/plane/.
4. Penner E.A., Shamanaev V.S. *Opt. Atmos. Okean.*, **7**, 338 (1994).
5. Balin U.S., Znamenskii I.V., Zuev V.E., Mel'nikov V.E., Samoilova S.V., Tikhomirov A.A. *Opt. Atmos. Okean.*, **8**, 1334 (1995).
6. Boreysho A.S., Volodenko V.A., Gryaznov N.A., Malamed E.R., Mendov Yu.N., Moshkov V.L., Pantaleev S.M., Pankratiev A.V., Finagin A.E., Chakchir S.Ya. *Proc. SPIE Int. Soc. Opt. Eng.*, **5479**, 177 (2004).
7. Boreysho A.S. *Kvantovaya Elektron.*, **35**, 393 (2005) [*Quantum Electron.*, **35**, 393 (2005)].
8. Killinger D.K., Menyuk N., DeFeo W.E. *Appl. Opt.*, **22** (5), 682 (1983).
9. Gordienko V.M., Putivskii Yu.A. *Kvantovaya Elektron.*, **21**, 284 (1994) [*Quantum Electron.*, **24**, 266 (1994)].
10. Wellstead S. *Fraktaly i vaivlety dlya szhatiya izobrazhenii v deistvii* (Fractals and Wavelets for Image Compression in Practice) (Moscow: Triumph, 2003).
11. Menzies R.T. *Appl. Opt.*, **10**, 1532 (1971).
12. Targ R., Steakley B.C., Hawley J.G., Ames L.L., Forney P., Swanson D., Stone R., Otto R.G., Zarifis V., Brockman P., Calloway R.S., Klein S.H., Robinson P.A. *Appl. Opt.*, **35**, 7117 (1996).
13. MacGovern A.J., Nahrstedt D.A., Johnson M.M. *Proc. SPIE Int. Soc. Opt. Eng.*, **4034**, 128 (2000).